International Journal of Earth, Energy and Environmental Sciences
ISSN: 2517-942X
Vol:14, No:7, 2020

Elasto-Plastic Behavior of Rock during Temperature Drop

N. Reppas, Y. L. Gui, B. Wetenhall, C. T. Davie, J. Ma

***Abstract*—**A theoretical constitutive model describing the stress-strain behavior of rock subjected to different confining pressures is presented. A bounding surface plastic model with hardening effects is proposed which includes the effect of temperature drop. The bounding surface is based on a mapping rule and the temperature effect on rock is controlled by Poisson's ratio. Validation of the results against available experimental data is also presented. The relation of deviatoric stress and axial strain is illustrated at different temperatures to analyze the effect of temperature decrease in terms of stiffness of the material.

***Keywords*—**Bounding surface, cooling of rock, plasticity model, rock deformation, elasto-plastic behavior.

I. Introduction

ROCKS contain micro-cracks and fractures and for this reason they are named fractured porous media. Thermo-hydro-mechanical models of rock are useful as the rock's stress-strain response is mainly controlled by initial porosity, porosity after the freezing of the rock, confining pressure, ice pressure which deforms the pores wall, shrinkage of the rock matrix, permeability, fracture density and stress-induced damage [1].

There have been several investigations in the last decades to describe the behavior of porous materials using the modified cap model [2], [3], cam-clay model [4], [5], bounding surface plasticity [6], [7] and hierarchical model [8] as well as many others. However, most of these models cannot capture the stress-strain response of fractured porous media under different confining pressures within changing temperature environment. The bounding surface model, which is adopted in this study, is a promising approach due to its simplicity. Dafalias and Popov firstly introduced the bounding surface plasticity for metal [9]. Then this theory was successfully extended to soil mechanics [10]-[12]. Fardis et al. introduced bounding plasticity to concrete [13]. In terms of its application to rocks, this is only found in [1], [14]. One missing parameter in the literature affecting the elastoplastic behavior of rock is temperature fluctuation. There are not enough numerical simulations and experimental data concerning freezing of rock to be applied to procedures like CO_2 injection.

In terms of the temperature influence on the stiffness of material, most of the undertaken research focused on heating the material to extreme temperatures. Few studies implement thermal effects on elastoplastic bounding surface design. Ultrasonic waves were used for Lanzhou Loess soil and an increase in the Young modulus and a decrease in the Poisson's ratio were found during a temperature drop from -1 ℃ to -10 ℃ [15]. Wu et al. [16] estimated the effects on Jiaozuo sandstone of temperature increase. The rock was heated from 20 ℃ to 100 ℃ and Poisson's ratio of the rock was found to increase while the Young modulus decreased [16]. Uniaxial compression tests using cryogen by [17] for rock specimens showed that the young modulus for different types of saturated rock like mudstone, conglomerate, rhyolite and schist decrease from 0% to almost 20% for a temperature increase from -15 ℃ to +15 ℃.

Reppas et al. [18] identified the lack in the literature of a fully robust hydro-mechanical model which includes thermal effects and suggested that the cooling of rock needs to be considered to simulate different procedures like CO_2 injection. Following the literature review and adopting the research [1], [12] as a basis, thermal effects were added to these models and the theoretical background was formulated.

The aim of this paper is to present an extensive and rigorous elasto-plastic constitutive model for rock material that includes effects on rock due to temperature drop. The introduction of the cooling effects can be the start point for following research on the elastoplastic behavior of rock materials during temperature decrease or freezing.

II. Plasticity Model

A. The Critical State Line

The critical state line (CSL) separates the brittle and ductile deformation in the $p' - q$ graph. p' is the current confining pressure and q is the deviatoric stress. Based on the Mohr-Coulomb model and introducing the frictional angle at critical state (ϕ'_{cs}), the slope of CSL (M_{cs}) can be expressed as [19]:

$$M_{cs} = \frac{6sin\phi'_{cs}}{\pm 3 - sin\phi'_{cs}} \quad (1)$$

The ($\pm$) is used to represent compressive loading by taking the positive symbol and extension by using the minus. The friction angle is the same in compression and tension but the value of (M_{cs}) is different.

The slope of the CSL (M_{cs}) as function of the lode angle (ϑ)

N. Reppas is a civil engineer and PhD student at the School of Engineering at Newcastle University, UK. (e-mail: N.Reppas2@newcastle.ac.uk).
Y.L. Gui is Senior Lecturer in Geotechnical engineering at Queensland University of Technology (QUT) (e-mail: yilin.gui@qut.edu.au).
B. Wetenhall is a Lecturer in Marine Engineering at the School of Engineering, Newcastle University, UK (e-mail: ben.wetenhall@ncl.ac.uk).
C.T. Davie is a Senior lecturer in Civil Engineering at the School of Engineering, Newcastle University, UK (e-mail: colin.davie@ncl.ac.uk)
J. Ma is an Associate Professor at School of Civil Engineering, Sun Yet-Sen University, Guangzhou, China (e-mail: majianjun@mail.sysu.edu.cn)

can be expressed as:

$$\vartheta = sin^{-1}\left[-\frac{3\sqrt{3}}{2}\frac{J_3}{\sqrt{J_2}}\right] \quad (2)$$

where $J_2 = \frac{1}{3}\cdot S_{ij}\cdot S_{ji}$ is the second invariant of deviatoric stress and $J_3 = det\boldsymbol{S} = \frac{1}{3}\cdot S_{ij}\cdot S_{jk}\cdot S_{ki}$ is the third invariant.

The Lode angle can vary from $+\frac{\pi}{6}$ for the maximum CSL slope (M_{csmax}) during compressive triaxial test to $-\frac{\pi}{6}$ for the minimum CSL slope (M_{csmin}) during a triaxial extensive test [20]. The slope of the CSL can be expressed in terms of Lode angle as [15], [20]:

$$M_{cs}(\vartheta) = M_{csmax}\left(\frac{2\Delta^4}{1+\Delta^4-(1-\Delta^4)sin3\vartheta}\right)^{\frac{1}{4}} \quad (3)$$

$$\Delta = \frac{M_{csmin}}{M_{csmax}} = \frac{3-sin\phi'_{cs}}{3+sin\phi'_{cs}} \quad (4)$$

In (3) if $\Delta = 1$ then the yield surface represents the Von-Mises Circle.

For critical state models, the elastic bulk modulus $\left(K^{el}_{bulk}\right)$ and elastic shear modulus (G^{el}) can be expressed by considering that the loading-unloading line occurs along a κ line in the $v - lnp'$ plane as follows:

$$K^{el}_{bulk} = \frac{v\cdot p'}{\kappa} \quad (5)$$

$$G^{el} = \frac{3(1-2n)}{2(1+n)}\cdot K^{el}_{bulk} \quad (6)$$

where $v = 1 + e$ is the specific volume; κ is the slope of the unloading-reloading line (URL) in a $v - lnp'$ diagram and n is Poisson's ratio. A schematic illustration of the isotropic compression line (ICL), critical state line (CSL), of the URL in the $v - lnp'$domain based on [19] presented in Fig. 1.

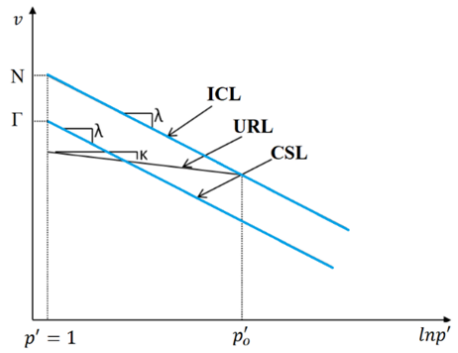

Fig. 1 Full representation of ICL, URL, CSL in the $v - lnp'$ space based on CSSM [1]

In Fig. 1, λ is the is the gradient of the isotropic compression line, N and Γ are the values of the specific volume for ICL and CSL, respectively at $p' = 1\,KPa\ or\ 1\,MPa$ and p'_o is the historic consolidated pressure (i.e. pre-consolidation pressure). The ICL is the loosest possible state that the rock can achieve for a specific mean effective stress.

B. Freezing Effects on Rock

Following the reverse pathway of [16] as we need to simulate the effect of cooling the rock, we can estimate the change in Young modulus and Poisson's ratio. It can be outlined from the results of [15]-[17] that after decreasing the temperature below zero, Poisson's ratio decreases whereas the Young modulus increases. It is noted that porosity also plays an important role.

Poisson's ratio will be influenced by temperature change so that for isotropic material:

$$n = n_{temp} \quad (7)$$

The bulk modulus can be expressed now as:

$$K_{matrix} = (1 + a\cdot\varphi)K_{porous} \quad (8)$$

where $a = [3(1 - n_{temp})]/[2(1 - 2n_{temp})]$ and φ is the porosity of the whole medium [21]. According to the value of the porosity, the bulk modulus of the porous and matrix can be calculated. For this research it is assumed that when the temperature is subzero, the whole amount of water in the porous medium is frozen. Also, it was assumed that the bulk and shear modulus of the whole porous domain can be expressed as:

$$K^{el}_{bulkf} = (1 - \varphi)K^{el}_{bulk} + \varphi(1 + a\varphi)K^{el}_{bulk} \quad (9)$$

$$G^{elf} = \frac{3(1-2n)}{2(1+n)}\cdot K^{el}_{bulkf} \quad (10)$$

for subzero temperatures.

C. Elastic-Plastic Behavior

The plastic behavior can be quantified by damage evolution and plastic flow [1], [22]. In this paper only the plastic behavior of the rock is considered for simplicity as the main purpose is to show the temperature effects on elastoplastic behavior of rock.

The strain rate consists of elastic and plastic parts as:

$$\dot{\boldsymbol{\varepsilon}} = \dot{\boldsymbol{\varepsilon}}^{el} + \dot{\boldsymbol{\varepsilon}}^{p} \quad (11)$$

where $\dot{\boldsymbol{\varepsilon}}^{el}$ is the elastic strain increment and $\dot{\boldsymbol{\varepsilon}}^{p}$ is the plastic strain rate.

The intrinsic elastic modulus matrix for undamaged material can be expressed differently according to the temperature of the rock as follows:

$$\boldsymbol{S}^e = \begin{cases} \begin{bmatrix} K^{el}_{bulk} & 0 \\ 0 & 3G^{el} \end{bmatrix}, T > freezing\ point \\ \begin{bmatrix} K^{el}_{bulkf} & 0 \\ 0 & 3G^{elf} \end{bmatrix}, T \le freezing\ point \end{cases} \quad (12)$$

The freezing point can vary according to the water that is

being used for the saturation of the rock e.g saline water.

D.Bounding Surface

The shape of the bounding surface is created by plotting the yield points in the $q-p'$space for different materials. The yielding points were plotted for different types of sandstones based on experimental research of [22]. Khalili et al.'s [12] proposed yield surface for granular soils based on Cam-Clay equations agrees with the results of the experimental work [22] on sandstone. Considering this agreement, the modified cam clay theory and bounding restriction were adopted in this study. The equation describing the bounding surface for different type of porous rock can be determined as:

$$f(\breve{p}', \breve{q}, \breve{p}_c') = \frac{\breve{q}}{M_{cs}\cdot \breve{p}'} - \left(\frac{ln(\breve{p}_c'/\breve{p}')}{lnR}\right)^{1/M} = 0 \qquad (13)$$

where $\breve{p}'$ is representing the current effective stress on the yield surface, $\breve{p}_c'$ controls the size of the bounding surface and is a function of the damage variable D and the plastic volumetric strain ε_v^p; M controls the shape of the bounding surface. For the value of 1 the yield function is reduced to the original Cam-Clay model; R is a material constant that represents the ratio between $\breve{p}_c'$ and the value of $\breve{p}'$ at the crossing point of the yield function f with the CSL in the $q-p'$ domain. The validation of the bounding surface compared to different experimental results [22] is presented in Fig. 2.

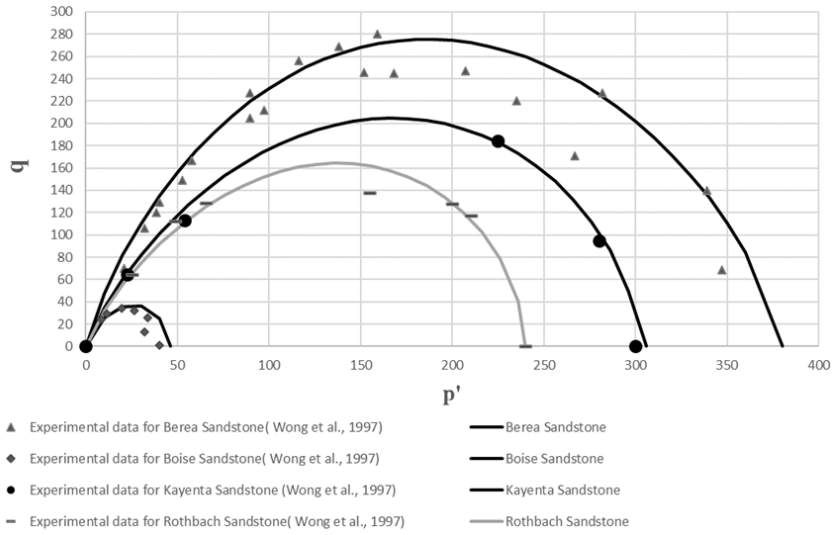

Fig. 2 Bounding surface validation

According to Khalili et al. [12], for plasticity, the incremental plastic stress-strain relationship is presented as:

$$\dot{\boldsymbol{\varepsilon}}^p = \frac{1}{h}\cdot \boldsymbol{x}\cdot \boldsymbol{n}^T \cdot \dot{\boldsymbol{\sigma}}' \qquad (14)$$

where $\boldsymbol{n} = [n_p \quad n_q]^T$ is the unit vector normal to loading surface at the current stress state $\boldsymbol{\sigma}'$ and $\boldsymbol{x} = [x_p \quad x_q]^T$ is the unit direction of the plastic flow at $\boldsymbol{\sigma}'$; h is the hardening modulus.

The unit normal vector $\boldsymbol{n} = [n_p \quad n_q]^T$ at the image point $\boldsymbol{\sigma}'$ is defining the direction of loading and can be given using the general equations of [12] as follows:

$$n_p = \pm \frac{-\breve{q}/(\breve{p}'[1-1/(Mln(\breve{p}_c'/\breve{p}'))])}{+\sqrt{\{-\breve{q}/(\breve{p}'[1-1/(Mln(\breve{p}_c'/\breve{p}'))])\}^2+1}} \qquad (15)$$

$$n_q = \pm \frac{1}{+\sqrt{\{-\breve{q}/(\breve{p}'[1-1/(Mln(\breve{p}_c'/\breve{p}'))])\}^2+1}} \qquad (16)$$

At any stress point $\boldsymbol{\sigma}'$ of a typical shape of plastic potential two vectors of plastic flow are identified one for compressive and one for extensive loading [12], [20].

E. Plastic Potential

The plastic potential $(g=0)$ is a factor of stress state and dilatancy factor (d). It expresses the ratio between the incremental plastic volumetric strain and incremental plastic shear strain. The dilatancy factor is positive for the opening or regeneration of micro-cracks and negative for closure. The forces acting for this procedure are the deviatoric stress and the hydrostatic stress. The plastic dilatancy [1], [12] can be expressed in terms of:

$$d = \frac{\dot{\varepsilon}_p^p}{\dot{\varepsilon}_q^p} = \frac{\partial g/\partial p'}{\partial g/\partial q} = M_d - \frac{q}{p'} \qquad (17)$$

where $M_d = (1+k_d\xi)M_{cs}$, and k_d is a material constant. M_d is used instead of M_{cs} to determine the dependency of d on density as indicated by k_d and ξ is a dimensionless parameter defined as the vertical distance between the current state and the CSL in the $v-lnp'$.

For porous rock, the plastic potential of granular soil [12] was adopted:

$$g(p', q, p_0) = q + (1 + k_d\xi)M_{cs}p' ln\frac{p'}{p'_o} \quad (18)$$

where p'_o is a dummy variable controlling the size of the plastic potential.

The components of $\boldsymbol{x} = [x_p, x_q]^T$ at $\boldsymbol{\sigma}'$ can be determined in a general form as:

$$x_p = \pm\frac{\partial g/\partial \boldsymbol{\sigma}'}{\|\partial g/\partial \boldsymbol{\sigma}'\|} = \pm\frac{d}{\sqrt{1+d^2}} \quad (19)$$

$$x_q = \pm\frac{\partial g/\partial \mathrm{q}}{\|\partial g/\partial \boldsymbol{\sigma}'\|} = \pm\frac{1}{\sqrt{1+d^2}} \quad (20)$$

The plasticity flow can be seen in Fig. 3.

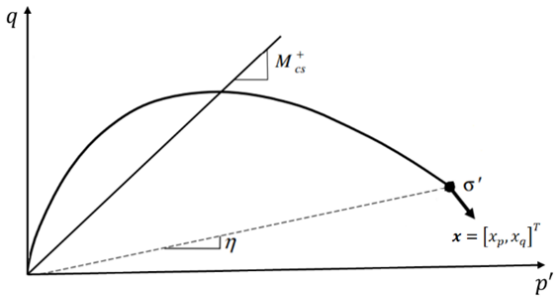

Fig. 3 Plasticity flow [12]

The stress-strain can be determined as:

$$\dot{\boldsymbol{\sigma}}' = \boldsymbol{S}^e - \frac{[\boldsymbol{S}^e]\cdot\boldsymbol{x}\cdot\boldsymbol{n}^T\cdot[\boldsymbol{S}^e]}{h+\boldsymbol{x}\cdot\boldsymbol{n}^T\cdot[\boldsymbol{S}^e]}\cdot\dot{\boldsymbol{\varepsilon}} \quad (21)$$

F. Plastic Hardening

Following the usual approach in bounding surface plasticity, the hardening modulus h is separated into two components, the plastic modulus h_b at stress point $\boldsymbol{\sigma}'$ and the arbitrary modulus h_f (the distance between the $\boldsymbol{\sigma}'$ and $\bar{\boldsymbol{\sigma}}'$):

$$h = h_b + h_f \quad (22)$$

Applying the plastic consistency condition at the bounding surface [20], and assuming that isotropic hardening of the bounding surface relates to isotropic damage and plastic compressive volumetric strain, h_b can be expressed as:

$$h_b = -\frac{\partial f}{\partial \breve{p}'_c}\left(\frac{\partial \breve{p}'_c}{\partial \varepsilon^p_p}\right)\frac{x_p}{\|\partial f/\partial \bar{\boldsymbol{\sigma}}'\|} \quad (23)$$

The arbitrary modulus h_f can be expressed based on the formulation proposed by [20] for sand and soil materials as:

$$h_f = \pm\left(\frac{\partial \breve{p}'_c}{\partial \varepsilon^p_p}\right)\frac{p'}{\breve{p}'_c}\left(\frac{\breve{p}'_c}{p'_c} - 1\right)m_p(\eta_p - \eta) \quad (24)$$

where $\breve{p}'_c$ and p'_c control the size of the bounding surface and the loading surface respectively, m_p being a material parameter and $\eta = \frac{q}{p'}$ is the stress ratio; $\eta_p = (1 - k\xi)M_{cs}$, with k being a material parameter. h_f is zero at bounding surface and infinite at the stress reversal point [12].

III. Parameter Identification

The constitutive parameters used for the elasto-plastic model are: κ, n to describe the elastic behavior; $\lambda, N, \Gamma, M_{cs}$ and p'_o to describe the CSL; M and R to define the shape of the bounding surface; m_p to calibrate the hardening modulus; k to define the peak strength line and k_d to define the stress-dilatancy relationship.

Assuming that elastic strains are negligible in comparison to plastic strains, k_d is obtained by plotting the stress ratio $\eta = \frac{q}{p'}$ against the measured dilatancy in standard drained triaxial compression test. The value of k can be obtained from the slope of η_p/M_{cs} versus ξ.

IV. Numerical Implementation

A. Mesh and Setup

The model was created using an axially symmetric mesh. The mesh consisted of 64 four-node quadrilateral elements with 2 by 2 integration points. A Finite Element Model (FEM) was implemented in MATLAB software [23]. One half of the sample was analyzed, and the boundary conditions are shown in Fig. 4. Modified Euler with automatic sub-stepping was adopted as an integration procedure in this study as the elastoplastic equations were strongly non-linear.

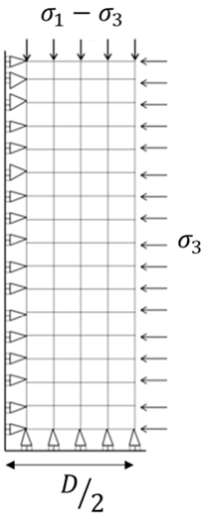

Fig. 4 The finite element mesh and boundary condition based on [1]

Validation of the proposed model to simulate the measured behavior of rock under monotonic loading was achieved by comparing numerical simulations with experimental results. In Figs. 5 and 6 also the behavior of rock at a different subzero temperature is presented.

The results are shown in Figs. 5 and 6. Discrete circles represent the experimental test data at room temperature (nearly 20 ℃) [23] and continuous solid and dashed lines are

the model predictions. It is important to note that the model results do not include damage. Sandstones were selected because of their wide range of porosity and grain size. Two different types of rock were simulated for a range of confining pressures.

B. Darley Dale Sandstone

Drained triaxial compressive tests were operated on Darley Dale sandstone (with a porosity of 13%) [24]. The diameter of the sample was 18.4 mm and the length was 38.1 mm. All samples were fully saturated. The axial strain speed was $1.3 \cdot 10^{-5}/s$. Results for three different confining pressures are presented (10, 50 and 100 MPa) with $\breve{p}_c' = 360\,MPa$. The model parameters are also presented in Table I.

TABLE I
MODEL PARAMETERS FOR DARLEY SANDSTONE

e	λ	κ	M_{cs}	N	R	k	m_p
0.38	0.15	0.0075	1.3	1.75	2.35	0.55	1

Poisson's ratio was set to $n = 0.25$. After the temperature drops below -5 ℃ , Poisson's ratio decreases. After the water in the rock is frozen, (9) and (10) are used for the calculation of the bulk and shear modulus.

Fig. 5 compares the model simulation and the experimental data at the same temperature for the response of the deviatoric stress-axial strain. It also shows an estimation of rock behavior for a certain temperature drop at -5 ℃.

The validation gives satisfying results. However, the damage of the material is not included and as a result for low confining pressures brittle behavior cannot be described perfectly. Damage of the material would influence the parameter κ which is the slope of the unloading-reloading line and that could set a limit on the increase of the deviatoric stress by increasing the axial strain of the material. However, the main purpose of this paper is to show the effect of temperature drop. Despite the absence of damage evolution in the model, it can be suggested that for low confining pressures the temperature influence is negligible. For high confining pressures the material when frozen is deformed at a certain level by applying less deviatoric stress. This is mainly occurring as for high confining pressures the material is acting as ductile.

C. Boise Sandstone

Boise sandstone with porosity of 35% is simulated [23]. The rock sample has a diameter of 18.4 mm and a length of 38.1 mm. Experiments are conducted at fixed pore water pressure of $10\,MPa$ under drained condition. The tested confining pressures are 10, 20, 100 and 200 MPa with $\breve{p}_c' = 450\,MPa$.The axial strain rate is $1.3 \cdot 10^{-5}/s$. The model parameters are also presented in Table II.

TABLE II
MODEL PARAMETERS FOR BOISE SANDSTONE

e	λ	κ	M_{cs}	N	R	k	m_p
0.5385	0.10	0.033	1.7	1.80	2.35	1	16

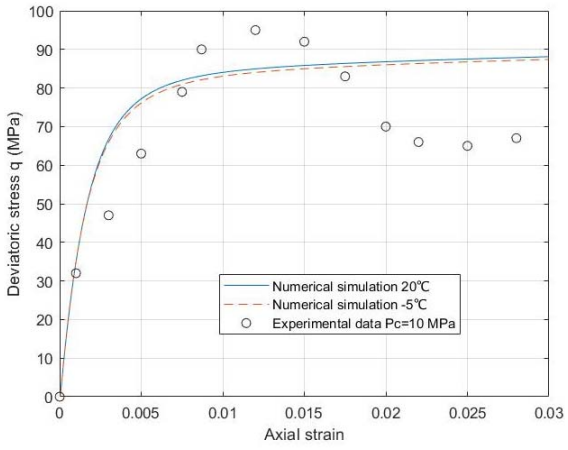

(a)

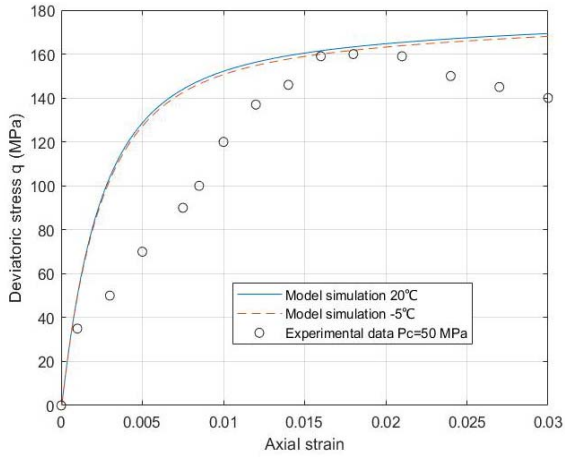

(b)

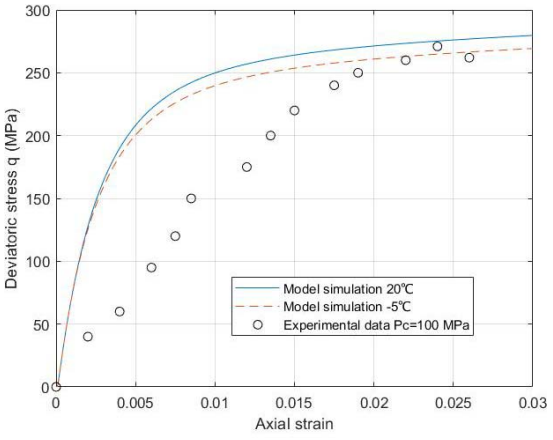

(c)

Fig. 5 Deviatoric stress-axial strain relationship at different confining pressures (a) Pc = 10 MPa, (b) Pc = 50 MPa, (c) Pc = 100 MPa at room temperature validated using experimental results and compared to -5 ℃ estimation

Fig. 6 shows the response of fully saturated Boise sandstone

under different confining pressures. The behavior of rock is well captured by the proposed model even though damage effects are neglected.

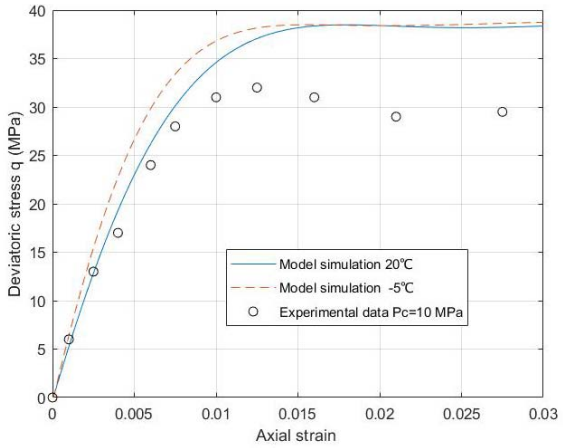

(a)

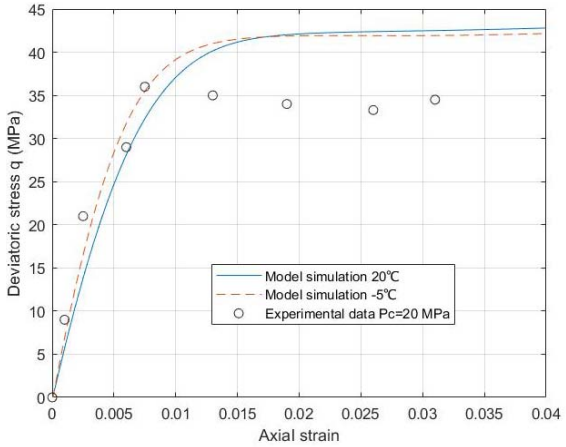

(b)

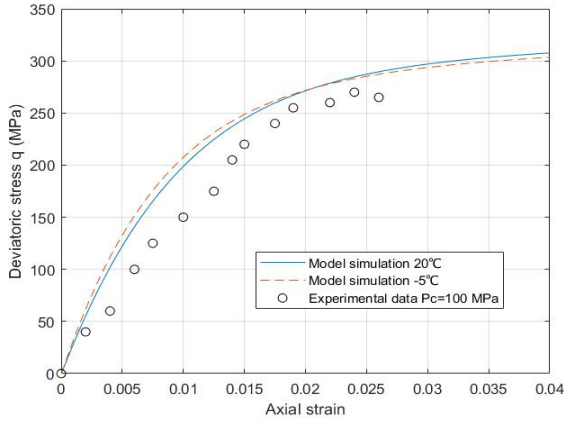

(c)

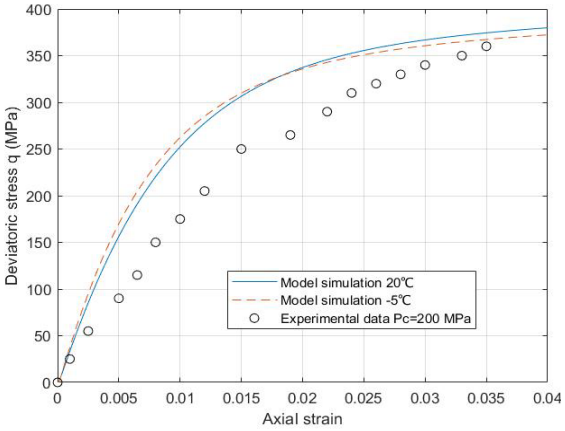

(d)

Fig.6 Deviatioric stress-axial strain with different confining pressures (a) Pc = 10 MPa, (b) Pc = 20 MPa, (c) Pc = 100 MPa, (d) Pc = 200 MPa at room temperature validated using experimental results and compared to -5 ℃

Comparing now the behavior at different temperatures, for low confining pressure the material needs more loading to deformed at a certain value. Consequently, for lower confining pressures (Pc $\leq$ 50 MPa) the material is becoming gradually stiffer as the temperature is decreasing. When the peak deviatoric stress is reached then according to Figs. 6 (a), (b) the behavior is almost the same. For high confining pressures, as the material is following the ductile pathway the differences are less. Nevertheless, it can be noticed that for lower axial strain the iced rock is behaving as stiffer whereas for higher axial strain ($\varepsilon_1 > 0.02$) the material is losing strength.

D.Temperature Drop at Different Confining Pressures

Based on the results of the two rocks (Darley Dale sandstone and Boise sandstone) it can be suggested that the porosity of the material especially for low subzero temperatures is significantly influencing the behavior of rock. This is happening especially for low confining pressures where brittle behavior exists. It should be mentioned that Poisson's ratio is mainly changing during the freezing of the rock according to the porosity of the material. For higher confining pressures and ductile behavior, temperature is not affecting stiffness much.

To better analyze the elastoplastic behavior of rock under different temperatures, simulations are presented for Boise Sandstone at different temperatures for two different confining pressures Pc = 10 MPa and Pc = 100MPa (Fig. 7). For these two simulations it was assumed that during temperature drop, Poisson's ratio is decreasing as the material is becoming stiffer and the elastic modulus is increasing. An important decrease in the Poisson's ratio is taking place after the freeze of the pores. Two graphs are provided for different temperatures to present how the deviatoric stress during a triaxial compressive test is changing due to temperature drop.

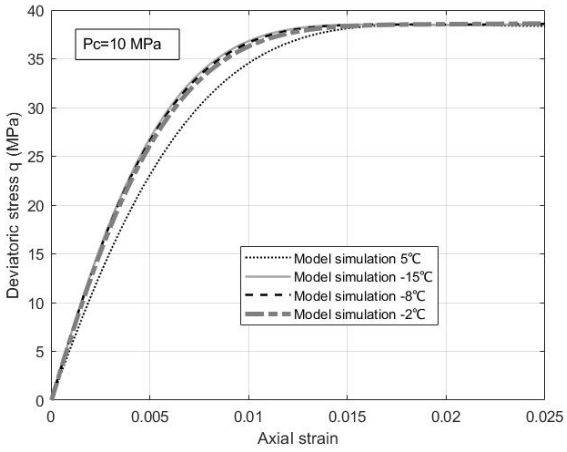

(a)

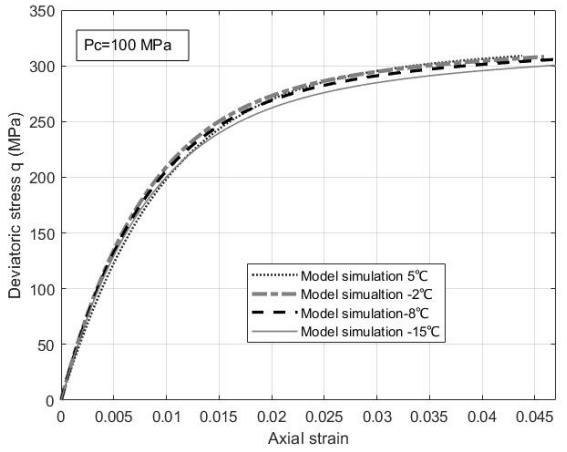

(b)

Fig. 7 Deviatoric stress-axial strain for Boise sandstone for (a) Pc = 10 MPa, (b) Pc = 100 MPa at different temperatures

It can be seen from Fig. 7 for Boise sandstone that for low and high confining pressures the behavior of rock is not similar. Specifically, for low confining pressure, as temperature drops the material is becoming stiffer and the same settlement is achieved for higher deviatoric stress. However, for high confining pressures, although for $\varepsilon_1 \leq 0.005$ temperature change is not affecting deformation for higher axial strain values, the material is becoming less stiff. The main parameter affecting the behavior for low and high confining pressure is Poisson's ratio.

V. Conclusion

A bounding surface plasticity constitutive model for monotonic loading is presented based on [1]. The model showed good agreement with experimental data. The temperature effect was also added to the model mainly in terms of a change of Poisson's ratio according to the temperature drop. For subzero temperatures, the porosity of the material had a significant role as for fully saturated material, water becomes ice. The aim of this paper was to present a preliminary research on how cooling of rock affects the elastoplastic behavior of the material.

Research is now taking place to implement damage effects on rock for a better approximation of experimental results. Experimental work is also scheduled to be done for the validation and better calibration of the numerical model. This can then give a tool for many applications like CO_2 injection procedures.

References

[1] MA, J. 2014. Coupled flow deformation analysis of fractured porous media subject to elasto-plastic damage. PhD thesis, The University of New South Wales.
[2] Sinha, T., Curtis, J. S., Hancock, B. C., Wassgren, C., 2010. A study on the sensitivity of drucker-prager cap model parameters during the decompression phase of powder compaction simulations. Powder Technology. In Press, Corrected Proof
[3] Khoei, A. R., Azami, A. R., Haeri, S. M., 2004. Implementation of plasticity-based models in dynamic analysis of earth and rockfill dams: A comparison of pastorzienkiewicz and cap models. Computers and Geotechnics. 31, 384-409
[4] Shah, K. R., 1997. An elasto-plastic constitutive model for brittle-ductile transition in porous rocks. International Journal of Rock Mechanics and Mining Sciences & Geomechanics Abstracts. 34, 367
[5] Bigoni, D., Piccolroaz, A., 2004. Yield criteria for quasibrittle and frictional materials. International Journal of Solids and Structures. 41, 2855-2878.
[6] Lü, P., Li, Q., Song, Y., 2004. Damage constitutive of concrete under uniaxial alternate tension-compression fatigue loading based on double bounding surfaces. International Journal of Solids and Structures. 41, 3151-3166.
[7] Montáns, F. J., 2000. Bounding surface plasticity model with extended masing behavior. Computer Methods in Applied Mechanics and Engineering. 182, 135-162
[8] Mortara, G., 2009. A hierarchical single yield surface for frictional materials. Computers and Geotechnics. 36, 960-967.
[9] Dafalias, Y. F., Popov, E. P., 1975. A model of nonlinearly hardening materials for complex loading. Acta Mechanica. 21, 173-192
[10] Dafalias YF, Herrmann LR. Bounding surface plasticity. II: application to isotropic cohesive soils. Journal of Engineering Mechanics 1986; 112(12):1263–1291.
[11] Bardet JP. Bounding surface plasticity for sands. Journal of Engineering Mechanics 1986; 112(11): 1198–1217
[12] Khalili, N., Habte, M. & Valliappan, S. 2005. A bounding surface plasticity model for cyclic loading of granular soils. *International journal for numerical methods in engineering,* 63**,** 1939-1960.
[13] Fardis, M. N., Alibe, B., Tassoulas, J. L., 1983. Monotonic and cyclic constitutive law for concrete. Journal of Engineering Mechanics. 109, 516-536.
[14] Guo, P. J., Wan, R. G., 1998. Modelling the cyclic behaviour of brittle materials using a bounding surface plasticity-damage model. International Journal of Rock Mechanics and Mining Sciences. 35, 437-438.
[15] Sheng, Y., Peng, W., Wen, Z. & Fukuda, M. Physical properties of frozen soils measured using ultrasonic techniques. Proceedings of 8th International Conference on Permafrost, 2003. 1035-1038.
[16] Wu, G., Wang, Y., Swift, G. & Chen, J. 2013.Laboratory Investigation of the Effects of Temperature on the Mechanical Properties of Sandstone. Geotechnical and Geological Engineering, 31.
[17] Aoki, K., Hibiya, K. & Yoshida, T. 1990. Storage of refrigerated liquefied gases in rock caverns: characteristics of rock under very low temperatures. Tunnelling and Underground Space Technology, 5, 319-325.
[18] Reppas, N., Gui, Y. L. & Wetenhall, B. 2019. A General Review on Rock Stability Due to CO2 Injection. 53rd U.S. Rock Mechanics/Geomechanics Symposium. New York City, New York: American Rock Mechanics Association.
[19] Wood, D. M. 1991. *Soil Behaviour and Critical State Soil Mechanics,* Cambridge, Cambridge University Press.
[20] Khalili, N., Habte, M. A. & Zargarbashi, S. 2008. A fully coupled flow

deformation model for cyclic analysis of unsaturated soils including hydraulic and mechanical hystereses. *Computers and Geotechnics,* 35**,** 872-889.
[21] Huang, S., Liu, Q., Liu, Y., Ye, Z. & Cheng, A. 2018. Freezing Strain Model for Estimating the Unfrozen Water Content of Saturated Rock under Low Temperature. *International Journal of Geomechanics,* 18**,** 04017137.
[22] Wong, T.-F., David, C. & Zhu, W. 1997. The transition from brittle faulting to cataclastic flow in porous sandstones: Mechanical deformation. *Journal of Geophysical Research: Solid Earth,* 102**,** 3009-3025.
[23] The Mathworks Inc., Matlab, R2020b [computer program], 2020
[24] Baud, P., Zhu, W. & Wong, T. F. 2000. Failure mode and weakening effect of water on sandstone. *Journal of Geophysical Research: Solid Earth,* 105, 16371-16389.

Nikolaos Reppas was born at Agrinion, Greece. He obtained his School Certificate (Apolyterion) from the 3rd General Lyceum of Agrinion, Greece with distinction He holds a Diploma (MEng) in Civil Engineering (5-year degree), conferred by the University of Patras, Greece (2017). He acquired a Master of Science Degree (MSc) in Geotechnical engineering, from the University of Dundee (2018). At the moment he is a PhD student at Newcastle University, UK. His research focuses on wellbore stability for carbon sequestration in geological formations.

Dr Yilin Gui joined the QUT in 2019 as a Senior Lecturer in Geotechnical Engineering. He was Lecturer in Geotechnical Engineering in Newcastle University, UK, and Research Fellow in Nanyang Technological University and Monash University. He obtained his PhD from UNSW Sydney and PG Certificate from Newcastle University, UK. He is a Fellow of Higher Education Academy. His research interests are focused on rock and soil mechanics, computational and constitutive modelling of geomaterials and Geo-environmental Engineering and other related areas in Geotechnical Engineering and Mining Engineering. His current research projects include THM in rock mechanics, environmental impact on soil structures and application of computation methods in Geotechnics.

Dr Ben Wetenhall is a lecturer at Newcastle University specializing in CO_2 transportation. He is a member of the Scientific Council of the UK Carbon Capture and Storage Research Council and has research awards from RCUK (EPSRC) and from industry (International Energy Agency) totaling over £250k.

Dr. Jianjun Ma received his Doctor degree in Civil Engineering from The University of New South Wales, Australia. He is working as an Associate Professor in Geotechnical Engineering at Sun Yat-Sen University, China. He is doing research and consulting in Geotechnical Engineering, including constitutive model (plasticity theory and continuum damage mechanics) and numerical analysis (coupled flow deformation analysis, FEM and Distinct Lattice Spring Model) in Geomechanics.

Dr Colin Davie joined Newcastle University in 2004 as part of the Geotechnical and Structural Engineering (GEST) Group in the School of Engineering. His research interests focus on the analysis of concrete exposed to high temperatures (with applications in nuclear power plant structures, fires in tunnels and buildings etc.) and multi-phase behavior of the ground, concerned with fluid flow, heat transfer, electrical conductivity etc. (with applications in slope stability, geological disposal of radioactive waste, ground source energy, rock slope stability etc.). His area of teaching revolves around geotechnics, geology and rock engineering for civil engineers and engineering geologists.